Core Flow Ingredients: sensitivity to geodynamo priors

Poster by Hannah F Rogers[1,2], Nicolas Gillet[1], Julien Aubert[3], and Mioara Mandea[2]

1 ISTerre, Université Grenoble Alpes, France; 2 CNES, Paris, France; 3 IPGP, Paris, France; ✉ hannah.rogers@univ-grenoble-alpes.fr

The inversion process to produce core surface flow models is underdetermined, thus requires additional information. It is possible to build this prior information from various advanced numerical geodynamo simulations, and several models describing the time evolution of the geomagnetic field exist. However, there is no clear overview of the relative importance of different 'ingredients' entering in the core flow inversion process or the robustness of the inferred flow features.
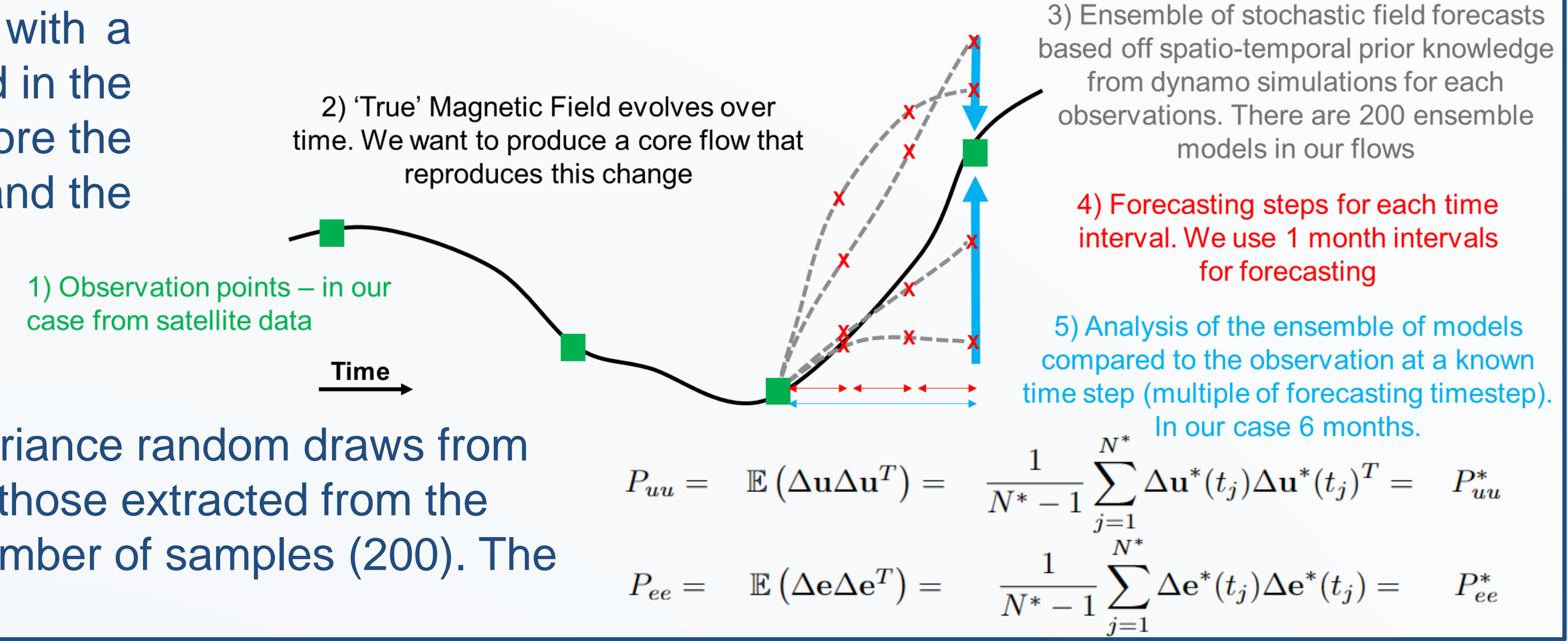
Methodology:

Pygeodyn is a python package for time-dependent stochastic flow inversion model with a Kalman filter: The time-evolution of the large scale potential magnetic field is described in the spectral domain by the radial induction equation: $\dot{\mathbf{b}} = A(\mathbf{b})\mathbf{u} + \mathbf{e}$, where $\dot{\mathbf{b}}$, $\mathbf{b}$, $\mathbf{u}$ and $\mathbf{e}$ store the spherical harmonic coefficients for the radial SV, the main field, the core surface flow and the errors of representativeness. Using an Euler-Maruyama scheme, their time integration take the form:

$$\mathbf{u}(t_{k+1}) = \mathbf{u}(t_k) - \Delta t^f D_u (\mathbf{u}(t_k) - \langle \mathbf{u} \rangle) + \sqrt{\Delta t^f} B_u \mathbf{w}_u(t_k)$$
$$\mathbf{e}(t_{k+1}) = \mathbf{e}(t_k) - \Delta t^f D_e (\mathbf{e}(t_k) - \langle \mathbf{e} \rangle) + \sqrt{\Delta t^f} B_e \mathbf{w}_e(t_k)$$

where D and B are the drift and diffusion matrices, and $\mathbf{w}$ are built from centred unit variance random draws from the 71p dynamo (Aubert and Gillet., 2021). The spatial covariances converge towards those extracted from the dynamo prior (see right). t_j is the number of dynamo samples (10000) and N* is the number of samples (200). The forecast timestep is 1 month and analysis occurs every 6 steps.

1) Observation points – in our case from satellite data

2) 'True' Magnetic Field evolves over time. We want to produce a core flow that reproduces this change

3) Ensemble of stochastic field forecasts based off spatio-temporal prior knowledge from dynamo simulations for each observations. There are 200 ensemble models in our flows

4) Forecasting steps for each time interval. We use 1 month intervals for forecasting

5) Analysis of the ensemble of models compared to the observation at a known time step (multiple of forecasting timestep). In our case 6 months.

$$P_{uu} = \mathbb{E}\left(\Delta u \Delta u^T\right) = \frac{1}{N^*-1}\sum_{j=1}^{N^*} \Delta \mathbf{u}^*(t_j)\Delta \mathbf{u}^*(t_j)^T = P_{uu}^*$$
$$P_{ee} = \mathbb{E}\left(\Delta e \Delta e^T\right) = \frac{1}{N^*-1}\sum_{j=1}^{N^*} \Delta \mathbf{e}^*(t_j)\Delta \mathbf{e}^*(t_j)^T = P_{ee}^*$$

Flow Models:

For investigating the effect of field model on the core surface flow inversion, we use three different magnetic field and SV models: Kalmag (Baerenzung et al., 2020); CHAOS-7 (Finlay et al., 2020); and COV-OBS-x2 (Huder et al. 2020). There is the potential to gain additional information by considering the SV to a higher maximum spherical harmonic degree than the main field, at least when continuous satellite data are available.
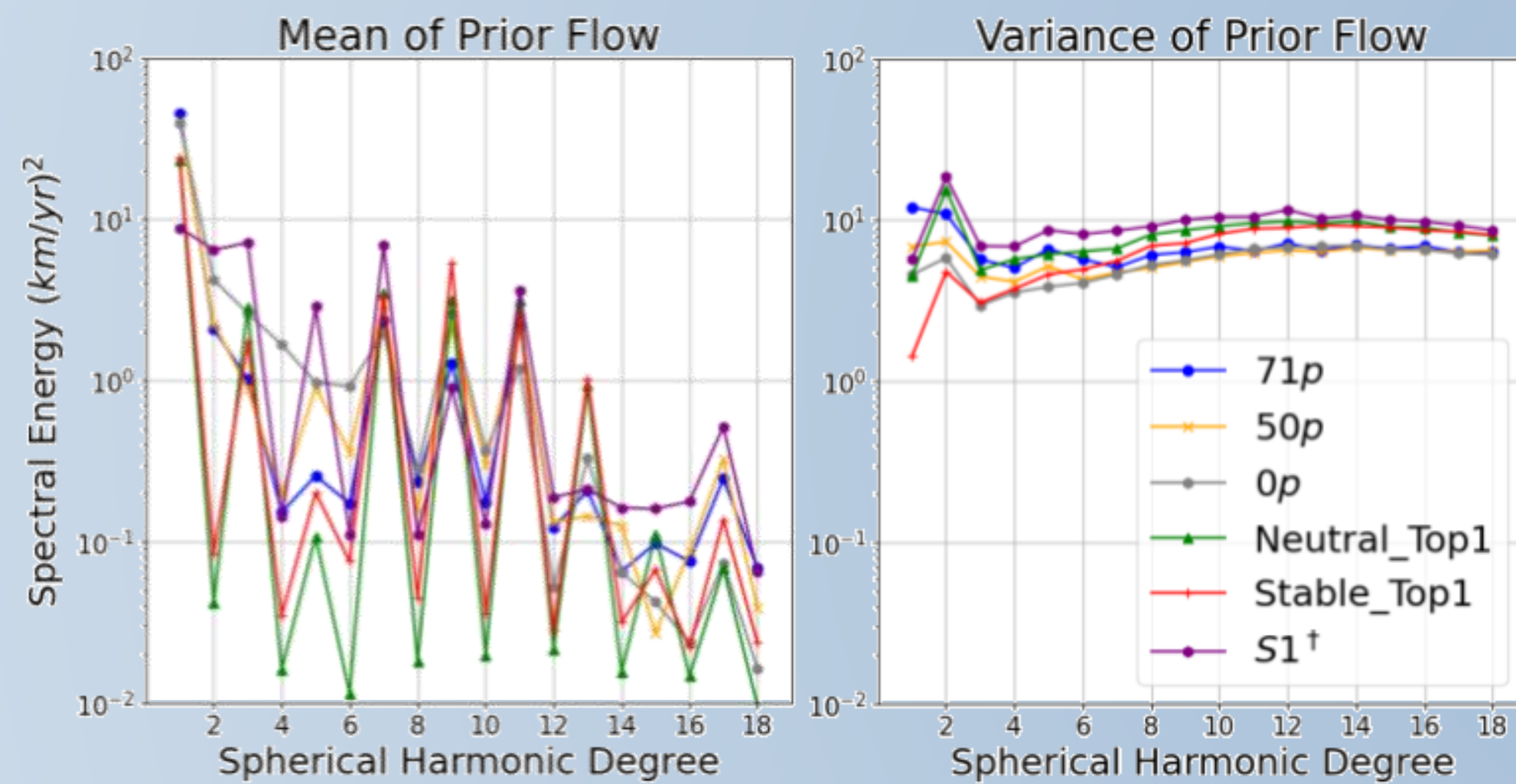
	L_B	L_{SV}	Time-span	prior	Treatment of Time
CHAOS-7	13	13, 16, 18	1999-2023	regularized	order 6 splines every 6 months
COV-OBS-x2	13	13	1880-2020	AR-2	order 4 splines every 2 years
Kalmag	13	13, 16, 18	1900-2023	AR-2	sequence of snapshots

Table above: Summary of the main characteristics considered for the three magnetic field models used in this study

	E_k	P_m	R_m	Al	Time-span	N_T	Γ_{EM}	Γ_G	Forcing
71p	3×10^{-10}	7.9×10^{-3}	1150	0.049	10000	50001	Y	Y	heterogeneous
50p	1×10^{-8}	4.5×10^{-2}	1100	0.114	20207.4	101037	Y	Y	heterogeneous
0p	3×10^{-5}	2.5	950	135360	135360	1505	Y	Y	heterogeneous
Neutral_top1	3×10^{-5}	4	1450	0.68	90530	9054	Y	Y	isotropic
Stable_top1	3×10^{-5}	4	1500	0.81	32200	3221	Y	Y	isotropic
S1[†]	1×10^{-6}	0.8	1800	0.26	12057	15328	N	N	isotropic
Earth	10^{-15}	$\sim 10^{-6}$	~ 1500	$\sim 10^{-2}$			?	?	?

*Table above: Relevant parameter values for each of the dynamos in the comparison, compared to Earth*

Fig right: Spatial power spectra for the time average flow (left) and the departure from this average (right) of each prior considered

Mean of Prior Flow — Variance of Prior Flow

- 71p
- 50p
- 0p
- Neutral_Top1
- Stable_Top1
- S1[†]

Spectral Energy $(km/yr)^2$ vs Spherical Harmonic Degree

Geodynamo Priors:

Calculating prior information from dynamo simulations requires long series, in order to describe enough independent configurations of the core flow. Considering a turn-over time in the core of the order of 100 yr, basing our statistics on ~ 100 independent states requires series spanning O(10) kyr. We consider 2 families of models: along the path starting from the Coupled-Earth/0p dynamo (Aubert et al. 2017); and across the path, where the E_k number is similar to 0p but with different forcing and starting points for the path.

Fig right: PDF of the largest zonal (left) and non-zonal (right) coefficients for the along path dynamos (top) and across the path (bottom). 0p and Neutral_top1 shown for reference

Main Symmetric Coefficients PDF — Main Assymmetric Coefficients PDF
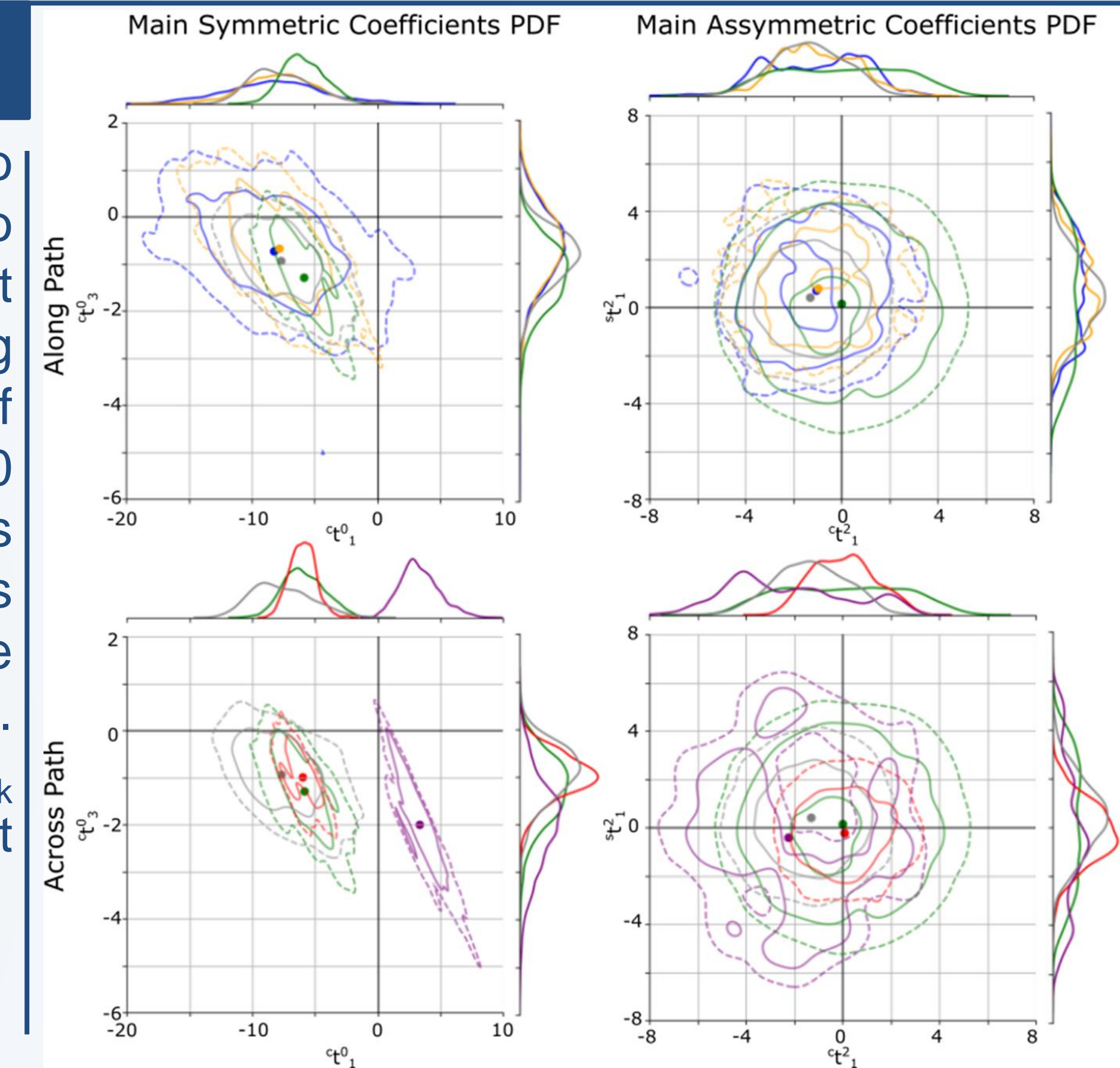
Results:

The results show that both the geodynamo prior and the choice of gauss coefficients used in the inversion do affect the resulting flow models. However, the effect of the choice of the prior has a greater impact on the flow compared to the choice of field model over the satellite era but the choice of the field model has a similar effect to the choice of prior in pre-satellite times. Increasing the time from the present increases the difference between the field models, leading to a greater impact when changing the field model. The choice of moving along the path is always a lesser effect than moving across the geodynamo path. Increasing the L_{SV} over the satellite era has a comparable effect to moving along the path in the satellite era but the large errors associated with higher degrees in the pre-satellite era minimises the difference seen when completing the flow inversion. The geodynamo prior affect the flow coefficients such as the large offset in the S1[†] flow coefficients variation in time for t_1^0 and $c_{t_2}^1$. The flow models converge in the satellite era. One of diagnostics we use is:

$$\chi(t) = \frac{\|\partial_t B_r\|}{\|\mathbf{u}_h\| \|\nabla_h B_r\| + \|B_r\| \|\nabla_h \cdot \mathbf{u}_h\|}$$

or for bandpassed values:

$$\partial_t \tilde{B}_r \simeq \tilde{\mathbf{u}}_h \cdot \nabla_h \hat{B}_r + \hat{B}_r \nabla_h \cdot \tilde{\mathbf{u}}_h + \hat{\mathbf{u}}_h \cdot \nabla_h \tilde{B}_r + \tilde{B}_r \nabla_h \cdot \hat{\mathbf{u}}_h$$

$$\tilde{\chi}(T) = \frac{\|\partial_t \tilde{B}_r\|_\tau}{\|\tilde{\mathbf{u}}_h\|_\tau \|\nabla_h \hat{B}_r\|_\tau + \|\hat{B}_r\|_\tau \|\nabla_h \cdot \tilde{\mathbf{u}}_h\|_\tau + \|\hat{\mathbf{u}}_h\|_\tau \|\nabla_h \tilde{B}_r\|_\tau + \|\tilde{B}_r\|_\tau \|\nabla_h \cdot \hat{\mathbf{u}}_h\|_\tau}$$

The figure below shows that there is greater observational constraint for the short-period flow dynamics than long-period. Instead, the null space for the flow inverse problem, where the solution is mostly determined by the prior, is wider towards long periods.

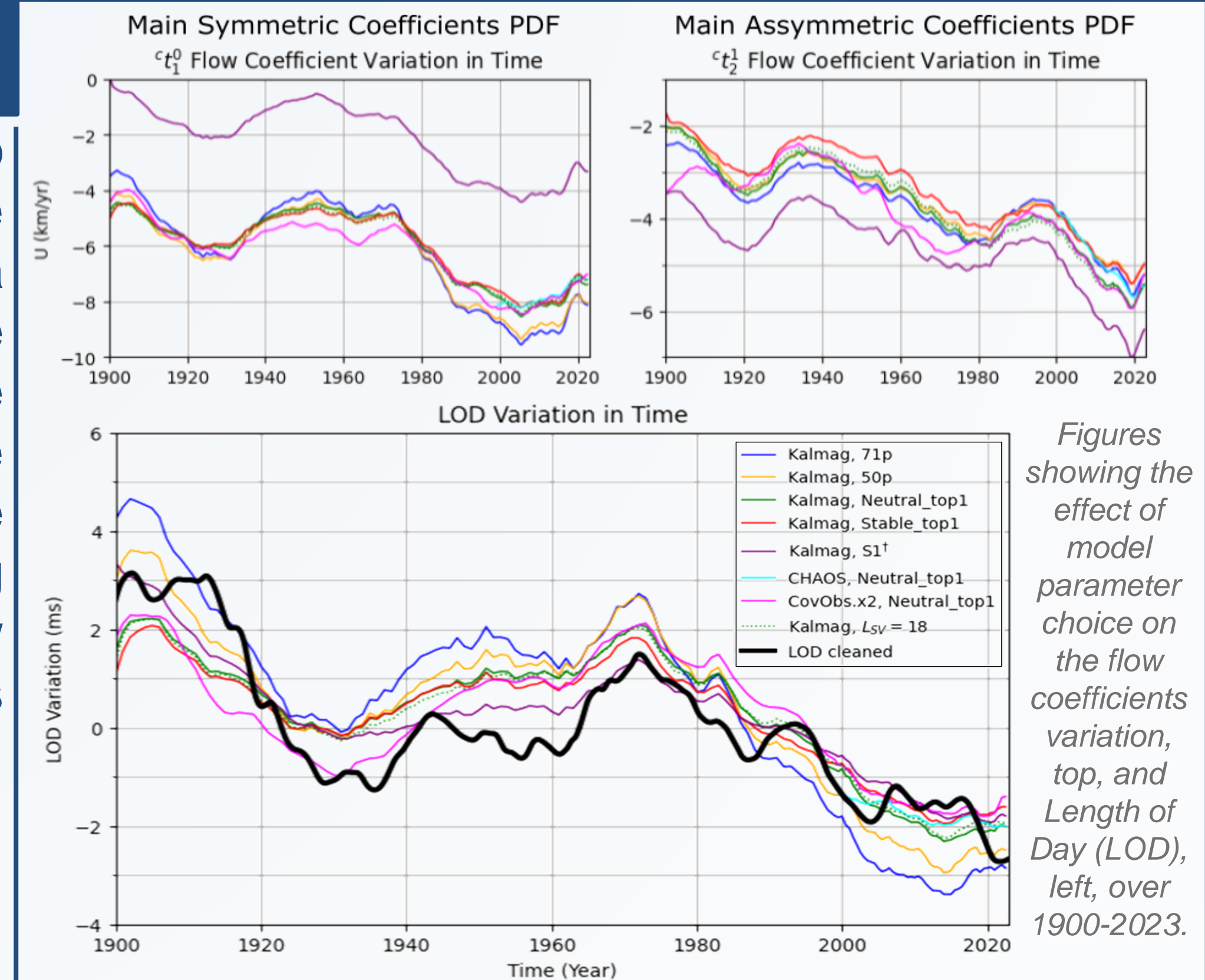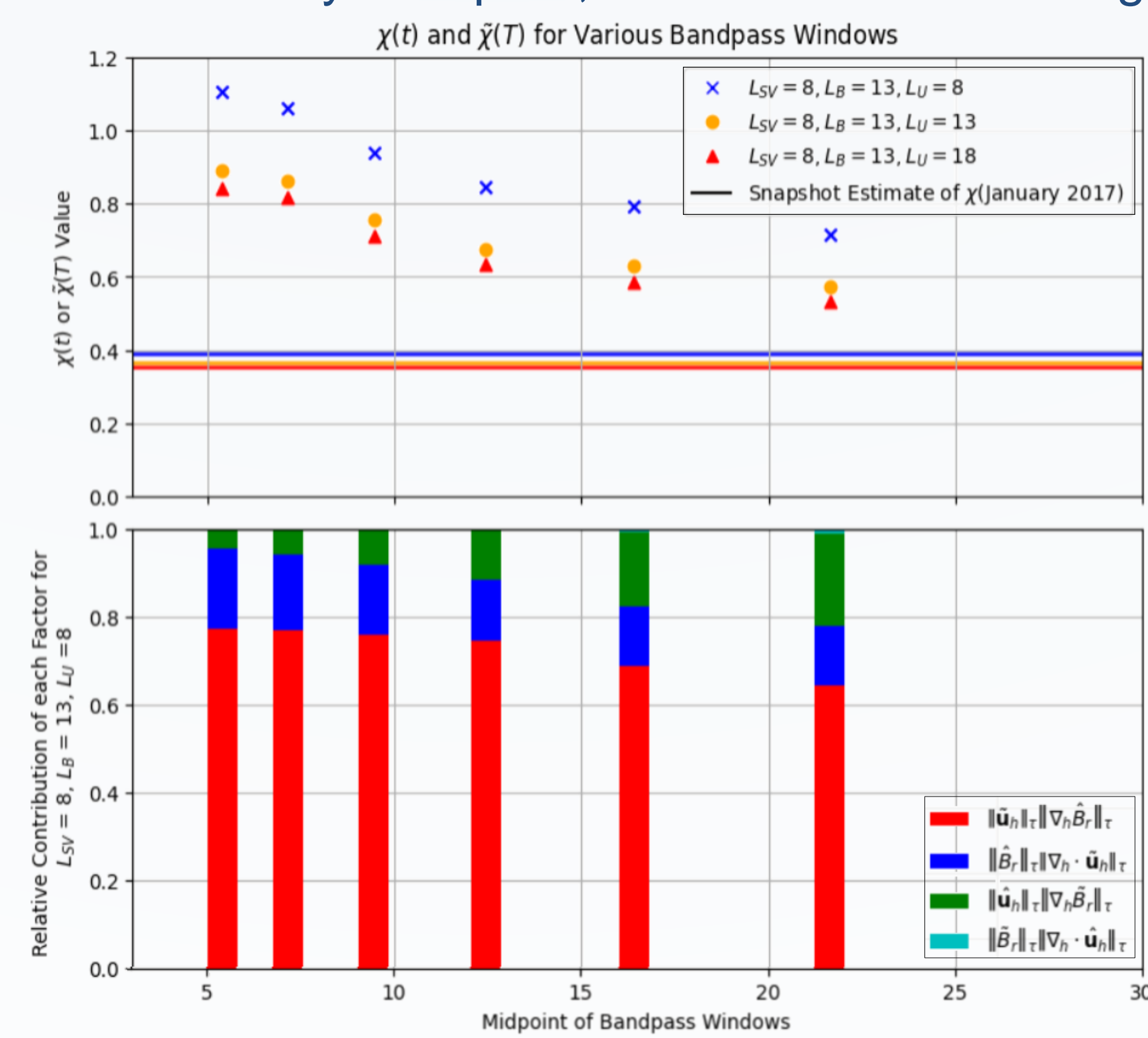| January 2017	CHAOS-7	Kalmag	CovObs.x2
71p prior *(Aubert and Gillet, 2021)*	7.5%	5.7%	6.7%
50p prior *(Aubert et al., 2017)*	8.0%	6.1%	7.4%
0p prior *(Aubert et al., 2013)*	7.7%	7.8%	8.7%
Neutral_top1 prior *(Aubert, pers comm)*	2.8%	**Reference**	1.6%
Stable_top1 prior *(Aubert, pers comm)*	11.9%	7.3%	8.9%
S1[†] prior *(Schwaiger et al., 2024)*	28.0%	23.7%	25.7%
Neutral_top1 prior, $L_{SV} = 16$	10.0%	7.7%	
Neutral_top1 prior, $L_{SV} = 18$	13.4%	8.2%	

January 1970	CHAOS-7	Kalmag	CovObs.x2
71p prior		6.3%	10.5%
50p prior		4.8%	12.0%
0p prior		8.9%	21.7%
Neutral_top1 prior		**Reference**	7.2%
Stable_top1 prior		8.5%	17.1%
S1[†] prior		22.4%	26.9%
Neutral_top1 prior, $L_{SV} = 16$		2.2%	
Neutral_top1 prior, $L_{SV} = 18$		2.7%	

January 1920	CHAOS-7	Kalmag	CovObs.x2
71p prior		6.8%	20.1%
50p prior		6.7%	20.2%
0p prior		12.9%	31.1%
Neutral_top1 prior		**Reference**	17.4%
Stable_top1 prior		10.6%	31.0%
S1[†] prior		25.4%	39.1%
Neutral_top1 prior, $L_{SV} = 16$		2.2%	
Neutral_top1 prior, $L_{SV} = 18$		2.6%	

Table left: Table showing the kinetic energy difference as a percentage of the reference. The reference model for each time period is the Kalmag, $L_{SV} = 13$, Neutral top1 prior

Fig right: plot to show the values of chi with various bandpass windows and cut-offs. The top plot shows how the $\chi(t)$ for a snapshot (January 2017) compared to the $\tilde{\chi}(T)$ for different bandpass windows and differing truncations. The bottom plot shows how the different contributions to $\tilde{\chi}(T)$ changes with the bandpass window

$\chi(t)$ and $\tilde{\chi}(T)$ for Various Bandpass Windows

- $L_{SV} = 8, L_B = 13, L_u = 8$
- $L_{SV} = 8, L_B = 13, L_u = 13$
- $L_{SV} = 8, L_B = 13, L_u = 18$
- Snapshot Estimate of χ(January 2017)

$\chi(t)$ or $\tilde{\chi}(T)$ Value vs Midpoint of Bandpass Windows

Relative Contribution of each Factor for $L_{SV} = 8, L_B = 13, L_u = 8$

- $\|\tilde{\mathbf{u}}_h\|_\tau \|\nabla_h \hat{B}_r\|_\tau$
- $\|\hat{B}_r\|_\tau \|\nabla_h \cdot \tilde{\mathbf{u}}_h\|_\tau$
- $\|\hat{\mathbf{u}}_h\|_\tau \|\nabla_h \tilde{B}_r\|_\tau$
- $\|\tilde{B}_r\|_\tau \|\nabla_h \cdot \hat{\mathbf{u}}_h\|_\tau$

Main Symmetric Coefficients PDF — $c_{t_1^0}$ Flow Coefficient Variation in Time

Main Assymmetric Coefficients PDF — $c_{t_2}^1$ Flow Coefficient Variation in Time

LOD Variation in Time

- Kalmag, 71p
- Kalmag, 50p
- Kalmag, Neutral_top1
- Kalmag, Stable_top1
- Kalmag, S1[†]
- CHAOS, Neutral_top1
- CovObs.x2, Neutral_top1
- Kalmag, $L_{SV} = 18$
- LOD cleaned

Figures showing the effect of model parameter choice on the flow coefficients variation, top, and Length of Day (LOD), left, over 1900-2023.

Reference: Kalmag, Neutral_Top1, $L_{SV} = 13$ — Kalmag, 71p — Kalmag, Neutral_Top1, $L_{SV} = 18$ — Kalmag, 50p — CHAOS-7, Neutral_Top1, $L_{SV} = 13$ — Kalmag, Stable_Top1 — COVOBS_x2, Neutral_Top1, $L_{SV} = 13$ — Kalmag, S1[†]

Changing Maximum L_{SV} / Changing Magnetic Field and SV model / Changing the Dynamo Prior
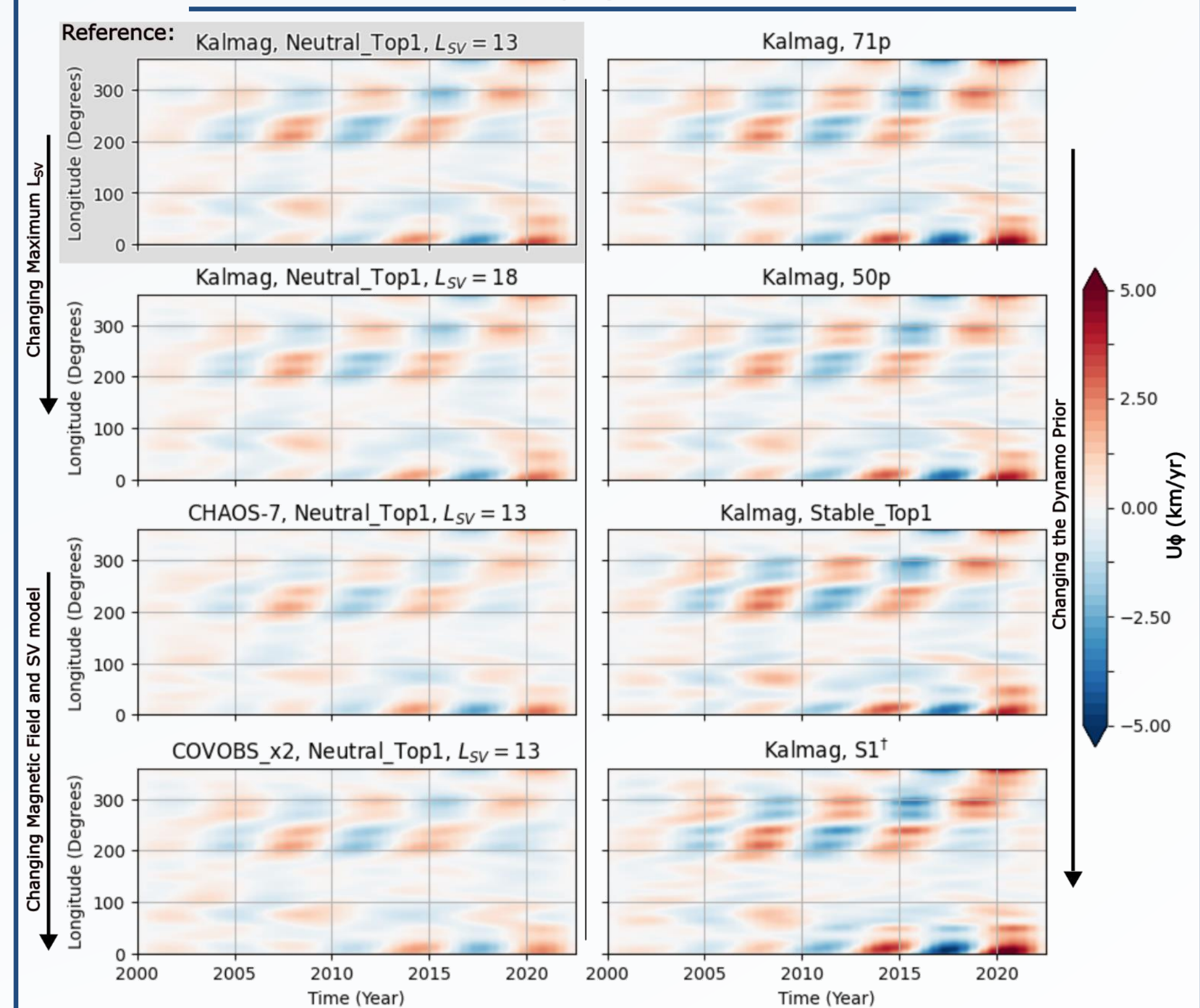
Fig above: Time-longitude plot of butterworth bandpassed flow motion at the equator for 4.5 – 9.5 years over the continuous satellite era (2000-2023). The structure of the flow is very similar but the bandpassed flow show different intensities and small spatial changes.

REFERENCES: **Aubert**, Finlay and Fournier (2013), Bottom-up control of geomagnetic secular variation by the Earth's inner core, Nature, doi:10.1038/nature12574; **Aubert**, Gastine and Fournier (2017), Spherical convective dynamos in the rapidly rotating asymptotic regime, JFM, doi:10.1017/jfm.2016.789; **Aubert and Gillet (2021)**, The interplay of fast waves and slow convection in geodynamo simulations nearing Earth's core conditions, GJI, doi:10.1093/gji/ggab054; **Baerenzung**, Holschneider, Wicht et al. (2020), The Kalmag model as a candidate for IGRF-13, EPS, doi:10.1186/s40623-020-01295-y; **Finlay**, Kloss, Olsen et al. (2020), The CHAOS-7 geomagnetic field model and observed changes in the South Atlantic Anomaly, EPS, doi:10.1186/s40623-020-01252-9; **Huder**, Gillet, Finlay et al. (2020), COV-OBS.x2: 180 years of geomagnetic field evolution from ground-based and satellite observations, EPS, doi:10.1186/s40623-020-01194-2; **Schwaiger**, Gillet, Jault et al. (2023), Wave-like motions and torques in Earth's core as inferred from geomagnetic data: A synthetic study, PEPI, doi:10.1016/j.pepi.2023.107104